Designing and Testing a Blended Wing Body with Boundary Layer Ingestion Nacelles

Melissa B. Carter[1], Richard L. Campbell[2], and Odis C. Pendergraft, Jr. [3]

NASA Langley Research Center, Hampton, VA 23681

Douglas M. Friedman[4] and Leonel Serrano[¶]

Boeing Phantom Works, Huntington Beach, CA 92647

A knowledge-based aerodynamic design method coupled with an unstructured grid Navier-Stokes flow solver was used to improve the propulsion/airframe integration for a Blended Wing Body with boundary-layer ingestion nacelles. A new zonal design capability was used that significantly reduced the time required to achieve a successful design for each nacelle and the elevon between them. A wind tunnel model was built with interchangeable parts reflecting the baseline and redesigned configurations and tested in the National Transonic Facility (NTF). Most of the testing was done at the cruise design conditions (Mach number = 0.85, Reynolds number = 75 million). In general, the predicted improvements in forces and moments as well as the changes in wing pressures between the baseline and redesign were confirmed by the wind tunnel results. The effectiveness of elevons between the nacelles was also predicted surprisingly well considering the crudeness in the modeling of the control surfaces in the flow code.

---

[1] Aerospace Engineer, Configuration Aerodynamics Branch, M/S 499, AIAA Member.
[2] Senior Research Engineer, Configuration Aerodynamics Branch, M/S 499, AIAA Associate Fellow.
[3] Aerospace Engineer, Configuration Aerodynamics Branch, M/S 499, AIAA Senior Member.
[§] Boeing Associate Technical Fellow, Flight Sciences, M/S H013-A319, AIAA Associate Fellow.
[¶] Aerospace Engineer, Flight Sciences, M/S H013-C328.

Nomenclature

c = local wing chord

C_D = drag coefficient

C_{fx} = stream-wise component of skin-friction coefficient

C_L = lift coefficient

C_m = moment coefficient

C_P = pressure coefficient

l = length of design station

L/D = lift-to-drag ratio

M_∞ = free-stream Mach number

Re_c = Reynolds number based on mean aerodynamic chord

x = distance in stream-wise direction

y = distance in span-wise direction

z = distance in vertical direction

α = angle of attack

η = wing semi-span station

I. Introduction

In the last decade, there has been a growing interest in the Blended Wing Body (BWB) concept as a way of addressing the rising cost of fuel, increasing number of air travelers, and environmental concerns such as emissions and noise. Recognizing the potential of this type of aircraft, NASA sponsored a study in 1994 to investigate the technical and commercial feasibility of the concept. This and other studies[1-4] have indicated fuel savings on the order of 30% for the BWB in comparison with other large aircraft (B747, A380), along with significant reductions in size and weight for a given mission. In addition to the reduced emissions associated with a lower fuel-burn rate, another environmental benefit would be a reduction in noise levels. Most of the configurations studied have engines mounted near the trailing edge on the upper surface of the wing, which tends to shield the inlet noise[5] and avoids the issue of exhaust noise reflecting off the lower surface of the wing, as with current large transports.

Although there are numerous benefits to the BWB configuration, some challenges have to be solved before the aircraft is viable. These issues include the elimination of the tail, a non-circular fuselage cross-section, and passenger comfort and safety. Significant progress has been made on many of these concerns and research on technologies applicable to a BWB continues within NASA and at the Boeing Company.

As noted above, most versions of the BWB have the engines mounted above the upper surface of the wing near the trailing edge. Even though initial configurations envisioned the engines mounted directly onto the wing surface, aircraft designers have focused their development efforts using pylon-mounted nacelles to avoid problems of surface integration and inlet flow distortion that comes from ingesting the boundary layer. Recent system studies indicated that boundary layer ingestion (BLI) inlet configurations could still lead to a number of benefits, including reduced ram drag, lower structural weight, and less wetted area than a strut-mounted engine configuration. References 2 and 6 indicate up to a 10% reduction in fuel burn could be achieved. However the propulsion/airframe integration (PAI) for the BLI nacelles would have to be improved and the flow distortion reduced to make the vehicle viable.

Several research efforts have addressed PAI and inlet distortion problems. Rodriguez[7] applied computational fluid dynamic (CFD)-based optimization to a 3-engine BWB/BLI configuration. His design reduced drag and improved inlet pressure recovery while holding distortion constant. Research has also been underway within the NASA Ultra-Efficient Engine Technology (UEET) Project to address both PAI and inlet flow distortion problems. In reference 8, active flow control (AFC) was applied to a generic BLI inlet/S-duct configuration to reduce flow distortion. In references 9 and 10, AFC installations were analyzed in CFD and the results of their studies indicate that significant improvements in inlet distortion levels can be obtained using pulsed-jet flow control. The UEET project funded this study to extend and apply advanced CFD-based design methods to the BLI PAI problem and to verify the results through high-Reynolds number tests in the National Transonic Facility (NTF). This study and its results are described in subsequent sections of this paper.

II. CFD Design and Analysis

A. Design Method Selection

The PAI design effort in this project was initiated because of encouraging results obtained during the NASA Advanced Subsonic Technology (AST) Program. In an unpublished study, the CDISC design method[11] coupled with

the OVERFLOW overset grid Navier-Stokes flow solver[12] (OVERDISC) was applied to an early twin-engine version of the BWB. The design modified the wing and the outer nacelle surfaces, although the nacelle-wing intersection had to be fixed due to grid movement difficulties. In spite of this restriction, OVERDISC nearly eliminated the PAI-related shocks and improved the lift/drag ratio by 6.5%.

Although the results indicated that the design method was efficient and effective, the initial grid generation and subsequent grid movement during the design proved to be cumbersome. Design methods based on unstructured grid flow solvers were tested on this configuration in hopes of eliminating the grid movement problems experienced with overlapping structured grids. Two unstructured tetrahedral grid Navier-Stokes flow solvers, each coupled with a different design approach, were selected for testing. The first was the USM3D flow solver[13], part of the TetrUSS software system[14], coupled with the CDISC design method. The second was the FUN3D flow solver that uses adjoint-based optimization for design[15]. A third option was to continue using OVERDISC and improve the grid movement method if the unstructured methods did not prove to be adequate.

A preliminary study was undertaken to evaluate the accuracy of the three flow solvers in predicting the flow characteristics for a clean-wing (no nacelles) version of the BWB that had been tested in the NTF in 1997.[10, 16] A photograph of that model is shown in Fig. 1. Since there was not a typical fuselage, a large fairing was created on top of the wing to cover the sting. The OVERDISC method was used to modify the fairing outer mold line to minimize the disturbance to the original wing pressures.[10]

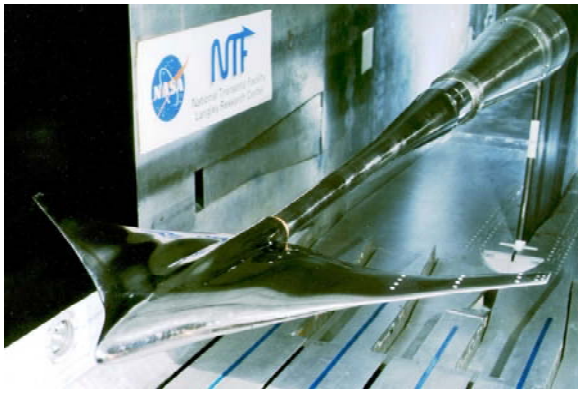

Figure 1 AST wing-only BWB model in NTF.

Each of the flow solvers (USM3D, FUN3D, and OVERFLOW) was run at a series of angles of attack at the cruise Mach number of 0.85 and a Reynolds number of 25 million for comparison with the wind tunnel data. A comparison of the USM3D results with experimental wing pressures at an inboard wing station near where a nacelle

would be located is given in Fig. 2. Generally, the computations matched the experimental data, and this correlation was typical for all span locations. The computed results indicate a slight acceleration ahead of the shock, but since there is no experimental data at that location, it is unclear how accurately the shock position and strength were matched, though there is good correlation downstream. Overall force and moment comparisons are shown in Fig. 3. The USM3D results correlated well with the experimental data. The levels are matched in and above the cruise range (C_L = 0.4-0.5) and even the pitch break was predicted fairly accurately.

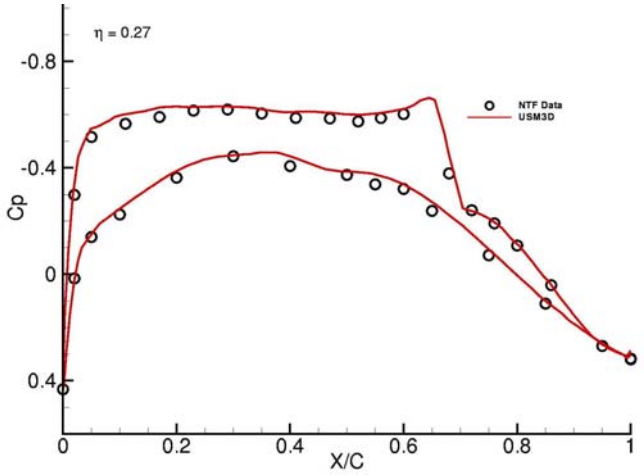

Figure 2 Correlation of CFD wing pressures with NTF data at cruise conditions.

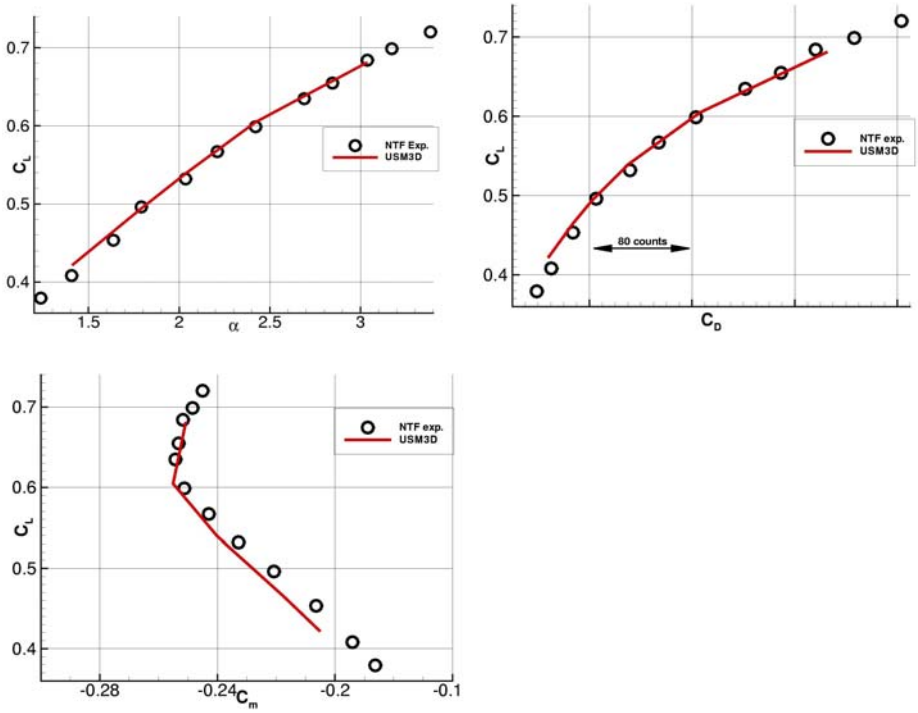

Figure 3 Correlation of CFD force and moment predictions with NTF data at cruise conditions.

The initial comparisons with experimental force and moment data for both FUN3D and OVERFLOW indicated that these correlations were worse than that with USM3D. Since the program schedule was tight, it was decided to proceed with USM3D/CDISC in the design phase. Subsequent investigations found that geometry and grid discrepancies led to the poor correlations with data for the other two codes.

B. Design Method Description

One additional benefit of selecting the USM3D/CDISC design system was the availability of a zonal design capability that had recently been implemented. This option allows a user to do local redesign using a subset of the full grid, which can significantly reduce the time required to develop a successful design strategy. This design system consisted of the PREDISC graphical pre/post-processor, codes for extracting and re-inserting the zonal design regions, the USM3D flow solver, the CDISC design module, and several auxiliary codes to link the flow solver and design module as described below.

1. USM3D Flow Solver

The zonal design process begins by running USM3D to obtain a flow solution for the full-grid baseline configuration at the design conditions. The USM3D code is a cell-centered, finite-volume Navier-Stokes flow solver that uses Roe flux-difference splitting[17] to compute inviscid flux quantities across the faces of the tetrahedral cells. Several options for turbulent closure are available: the one-equation Spalart-Allmaras (S-A) model[18] (with and without a wall function), and several two-equation models, including Menter's Shear Stress Transport (SST) model[19]. The parallel version of the flow solver was run in the implicit mode for this study. The wall function option with the S-A turbulence model was used to reduce the number of grid points required to model the boundary layer, and the minmod limiter was turned on to help stabilize the code during the design process (subsequent work indicates that the limiter probably was not needed). The code was modified to include a new boundary condition type for use on the zonal grid box faces. Setting this boundary condition type freezes current flow conditions on the zonal faces and at the corresponding ghost cell centers.

2. Zonal Grid Extraction

The grid and resulting solution files from USM3D are read into PREDISC where the user graphically defines the zonal region of interest. The shape of the region is currently limited to a rectangular box. Once the box is defined,

the extraction code identifies all cells that are completely within the box and marks the new zonal faces. The code then renumbers the new points, cells, and faces and writes out all files needed to run the zonal case (grid, restart, connectivity, etc.). A point/cell/face-mapping file is also saved to allow the modified zonal grid and/or restart files to be reinserted into the original full grid files after design. The zonal grid is often smaller then the full grid by an order of magnitude or more and it consequently requires fewer processors.

3. CDISC Design Method

After the zonal grid is extracted, PREDISC is used to select the components and surfaces for design and to define the locations and types of design stations. Design stations can be defined along surface patch boundaries or at the intersection of a user-defined plane and the surface. Stations may be distributed across a component as a series of parallel or radial planes. PREDISC extracts and displays the current surface geometry and pressure distribution at each design station. Additionally, the user can evaluate different design strategies by first combining various flow and geometry constraints, then running CDISC, and finally plotting the resulting target pressures and design geometries. This process is an automated option in PREDISC.

The CDISC module is a knowledge-based design method that has been coupled with a variety of 2-D and 3-D flow solvers and has been used with structured, overset, and unstructured grids. CDISC uses specified flow/geometry relationships developed from analytical or empirical studies to compute geometry changes based on the difference between current and target flow quantities. This eliminates the need to compute sensitivity derivatives and allows the design to converge in parallel with the flow solution, greatly reducing the time required for a design. The design time is further reduced by using flow constraints to automatically develop the target distribution from the current values of flow quantities such as pressure or skin-friction coefficients. These constraints address common engineering design variables such as span load, shock strength, section lift and pitching moment coefficients. Since this approach reduces problems such as an incorrectly specified pressure level, it is generally more robust than manually specifying a fixed input target. In addition to the flow constraints, geometry constraints such as thickness, curvature, volume and leading edge radius are available to address requirements from other disciplines such as structures and manufacturing.

4. Grid Modification

After CDISC determines the geometry changes at the design stations, the CFD grid is modified by two different codes. The first code performs a linear lofting of the changes at the design stations onto the previous surface grid, with special provisions for absorbing changes on a component with a single design station (e.g., adjust the fuselage grid for changes to the wing/fuselage intersection). The second code adjusts the volume grid to accommodate these changes. This process has proved more robust if the changes are made with respect to the original grid and design surface geometries.

For volume grid adjustment, the grid points are assigned to layers, with the first layer being points on a solid geometry surface, the second layer consisting of points connected to the points on the first layer, and so forth until all points are labeled. The movement of each point is determined by the displacement of the nearest point in the previous layer, with a decay function applied to points outside the boundary layer region. This initial movement can create cells with negative volumes and/or large volume differences between cells with a common face. The code will adjust these cells in an attempt to eliminate negative volume cells. Renormalizing the grid in the boundary layer region and adjusting cells with a common face so that the ratio of their volumes is less than a specified value are additional options. After the grid is successfully modified, it is returned to the flow solver for further analysis by restarting from the previous solution.

The design process described in the sections above is typically repeated for 10-20 cycles and the results evaluated using PREDISC. If the results are stable and converged, and the desired flow improvements were obtained with a reasonable surface geometry, the new zonal grid can be reinserted into the full grid for further analysis to confirm the global impact of the design. If needed, additional design work can be carried out on the full configuration using the design strategy developed using the zonal approach.

C. Grid Convergence Study

For the PAI design, a 3-engine, 450-passenger version of the BWB was chosen as a baseline. A semi-span unstructured grid consisting of about 4 million tetrahedral cells was generated using VGRID[20], part of the TetrUSS software system. The surface grid, mirrored to illustrate the full configuration, is shown in Fig. 4, with a close-up view of the nacelle area on the right-hand side of the figure. The original grid was generated using a powered-nacelle geometry provided by Boeing. Since the wind tunnel validation tests would use flow-through nacelles, the

grid was modified using PREDISC and other codes to increase the nacelle exit area so that the desired cruise mass flow ratio of about 0.72 was recovered.

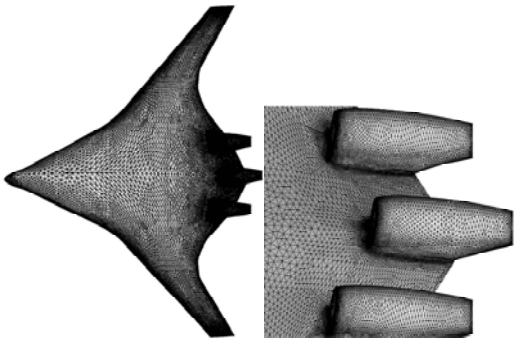

Figure 4 Unstructured Grid for BWB with BLI Nacelles

In order to ensure that the computational model of the aircraft was sufficient for capturing the BWB's flow characteristics, a grid convergence study was conducted. In order to test the suitability of the original grid, a second grid was generated that had the same surface geometry but had twice the surface resolution and total number of grid cells. Both grids were run at the cruise condition of Mach 0.85, angle of attack of 4-degrees, and a Reynolds number of 75 million. In order to determine grid convergence, the changes in the lift, drag and moment coefficients between the two grids were calculated (Table 1). These differences were minimal and thus confirmed that the original coarser grid was adequate for design and analysis, hence saving computer time and power.

Force	Change Between Grids
C_L	1.835E-03
C_D	1.42E-05
C_m	3.705E-04

Table 1 Change in Forces from Grid Convergence Study.

D. PAI Design Approach

Results from the USM3D flow analysis of the original coarser grid (Fig. 5) revealed several areas where the flow characteristics could be improved. In Fig. 5a, a weak-to-moderate shock can be seen near the lip of each nacelle. For the outboard nacelle, the shock is stronger on the inboard side, suggesting that a re-alignment of that nacelle along with some re-contouring of the nacelle/wing fairings should reduce wave drag. Fig. 5b shows a plot of contours of a function indicating the condition of the boundary layer in the region of the nacelles (referred to as the SEP or separation function). This function is based on levels of the stream-wise component of the skin-friction coefficient

and indicates areas of weak boundary layer with mild spanwise turning of the flow, $C_{fx} \leq 0.0005$ (green), incipient separation with strongly turning flow, $C_{fx} \leq 0.0002$ (yellow), and separation with reverse flow, $C_{fx} < 0.0$ (red). As shown in Fig. 5b, significant areas of separation are present ahead of each inlet, with weakened boundary layer flow spilling around and contaminating the flow over the elevon in between the nacelles. Reducing the separation on the elevon should provide a profile drag benefit and may improve the effectiveness of this control surface.

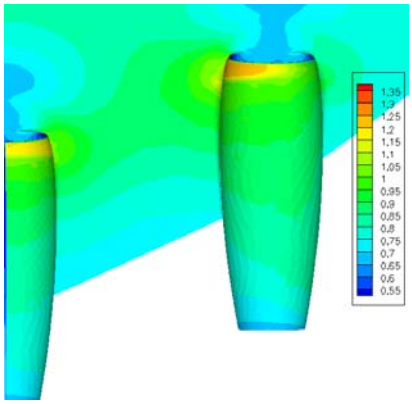

a) Mach

QuickTime™ and a
TIFF (LZW) decompressor
are needed to see this picture.

C_{fx} Levels:
0.0005
0.0002
< 0.0000

b) SEP function

Figure 5 Flow contours from initial USM3D analysis at cruise conditions.

It was decided to first use PREDISC to manually adjust the outboard nacelle cant angle and smooth the fairings around the base of each nacelle before proceeding to a CDISC-based design. A tow-out angle of 3 degrees gave similar, very weak shocks on each side of the outboard nacelle and, along with the smoothing, reduced the maximum local Mach number on the nacelles to less than 1.08. In addition to reducing the wave drag, the weakening of the shocks had a favorable effect on the boundary layer on the wing between the nacelles.

Using this new geometry as a starting point, a 3-zone CDISC design was initiated. Zonal boxes were defined around each of the nacelles and the elevon using sizing criteria from Ref. 21. Because the design runs were made using only the grid cells contained in each zonal box, design times were reduced by factors of 5, 3 and 20 for the inboard, outboard and elevon zones, respectively. This proved to be extremely useful since a number of design runs were required to refine the design strategy for each of the components. The general design approach was to reduce the size of the separated flow regions in front of each of the inlets, then plug these results back into the full grid and update the flow solution so that any improvements in the flow spilling around the nacelles would be reflected in the flow over the elevon. The central zonal grid would then be extracted for design of the elevon surface to improve any remaining flow problems.

There are several approaches available in CDISC for addressing separated flow, depending on the source of the adverse pressure gradient that causes it. For cases where the pressure field from a leading-edge attachment line slows the flow on an intersecting surface (e.g., wing/fuselage intersection), there are options in CDISC to grow a planform fillet or "horn" on the wing leading edge. If the separation is due to a strong shock on an airfoil section, a combination of flow constraints can be used to reduce the shock Mach number while maintaining lift. Constraints have also been developed to adjust pitching moment via aft loading to limit airfoil trailing edge separation. Finally, if the separation is due to an adverse pressure gradient caused by a local surface bump or component interaction away from a leading or trailing edge, constraints that limit and smooth local surface pressures and/or curvatures have proven effective.

In all of the approaches above, the skin friction characteristics on a surface are indirectly addressed through the application of pressure-based constraints. There is also a capability in CDISC based on the work of Green[22] that modifies a surface directly based on the difference between the current skin-friction distribution and a target distribution. Though more direct than the pressure-based constraints, this approach has been found to be much slower since more flow iterations were required per design cycle to adequately reflect the skin friction change rather than a pressure change resulting from a given geometry modification. In view of this, pressure-based constraints were selected for this study, with the specific approach illustrated in the next section.

D. CDISC Design Results

The CDISC design was initiated using the zonal grid containing the inboard nacelle. Although some of the flow separation in front of the inlet is related to the lip attachment line pressures, there is also a significant influence of

the reduced flow velocities in the duct itself. Therefore it was decided to try to reduce the flow separation by limiting the pressure levels on the wing surface approaching the inlet. A series of stream-wise design stations were defined that extended from the inlet to the rear wing spar approximately 2 nacelle diameters ahead of the inlet. Several of the design stations actually extended into the inlet in an effort to reduce the region of separated flow there. Figure 6 shows that the regions of weak boundary layer and flow separation ahead of the nacelles correlated fairly well with the pressure coefficients greater than 0.2. Note that the baseline SEP function levels in Fig. 5b differ from those in Fig. 6a because the latter results include the effects of the minmod limiter in USM3D. The minmod limiter was invoked to improve convergence during the design. The target pressure constraint strategy illustrated in Fig. 7 was formulated based on this Cp-SEP correlation. First, the stream-wise location where the pressure coefficient is first greater than 0.2 is determined and a pressure level constraint is implemented to keep the C_P less than 0.2 for a distance of x/l=0.1 aft of that point. A small region of neutral pressure gradient has been found beneficial in controlling the boundary layer growth before the trailing-edge pressure recovery on supercritical airfoils. Next, the target pressures are defined to be linear between this point and the current trailing edge value, then the target distribution is smoothed aft of x/l=0.5. In keeping with the recommendations of Ref. 21, the active design region began at x/l=0.2 and geometry smoothing was applied to control any kinks that may tend to form at the beginning of a partial-chord design region. Each successive design cycle develops a new target pressure distribution by applying the same constraint strategy to the current analysis pressures, except that the original location of the first occurrence of C_P=0.2 is always used.

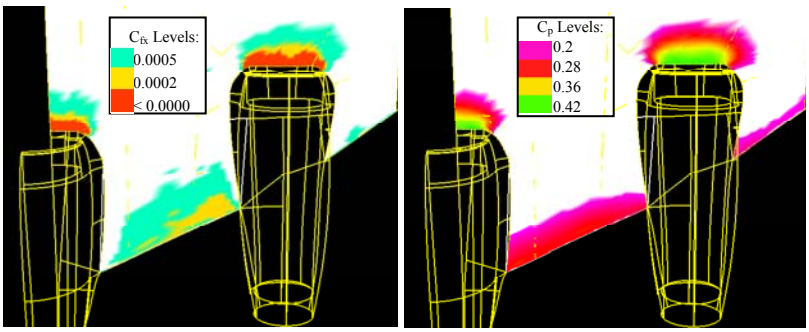

a) SEP function **b) Cp > 0.2 contours**

Figure 6 Correlation of boundary layer SEP function with pressure coefficient contours.

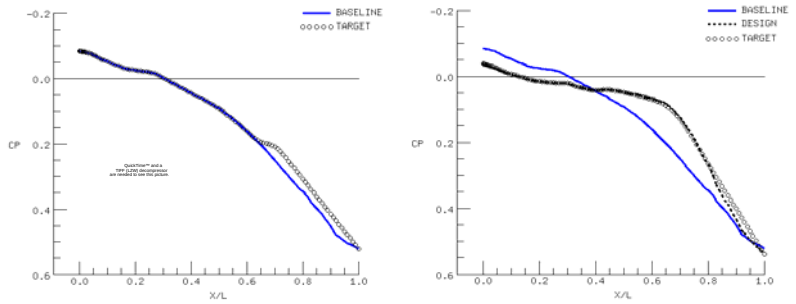

a) Initial **b) Final**

Figure 7 Target Pressure distributions for inboard nacelle design stations.

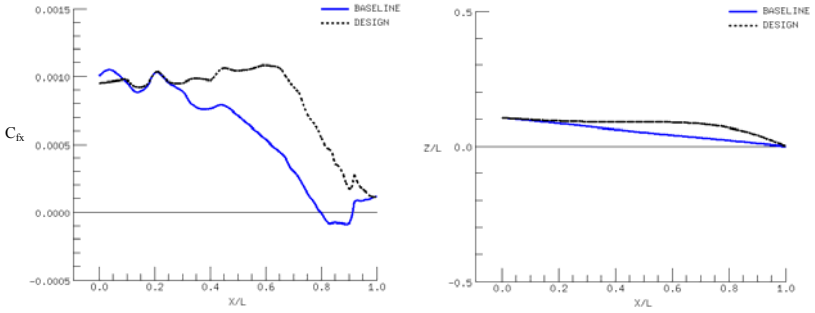

a) Skin-friction **b) Geometry**

Figure 8 CDISC design results for inboard nacelle design station.

The results for a design station going just inside the center nacelle are shown in Fig. 7b and 8. The x/L shown in figures 7 and 8 define 0.0 as the beginning of the design station and 1.0 as the downstream end. The final design pressure coefficients generally matched the target distribution and maintained lower values relative to the baseline over the aft end of the design region. There was concern that, although the milder pressure gradient in the region between x/l=0.4 and 0.7 should improve the local skin friction levels, the steeper adverse pressure gradient aft of that region could worsen the separation going into the inlet. This was not the case, as illustrated in Fig. 8a; instead, there was a significant increase in the skin friction level from x/l=0.3 aft. As also shown in Fig. 9a, the regions of reverse flow and most of the incipient separation has been eliminated and there is some improvement in the boundary layer health over the inboard side of the elevon. Please note that Fig. 9a shows the results from the flow solver after the zones were reinserted into the grid. Figure 8b shows that a bump was created above the original surface to produce these changes. It should be noted that this bump does not function as a diverter, but simply improves the flow characteristics of the boundary layer that is ingested.

The same general design strategy was used for the outboard nacelle zone. Although the boundary layer characteristics were improved, the change was not as dramatic as for the inboard nacelle. This is probably due to the shorter design region available since the rear wing spar is about a nacelle diameter closer to this inlet than to the inboard inlet. Nevertheless, the modifications ahead of the inlet, combined with the effects of reducing the nacelle shock by toeing the nacelle out, nearly eliminated the incipient separation region on the outboard portion of the elevon.

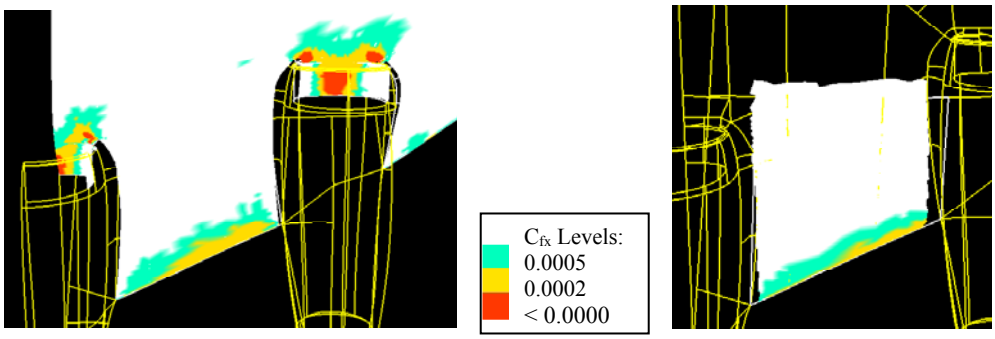

a) Full-grid analysis of final design. **b) Zonal-grid analysis of elevon design**

Figure 9 SEP function contours.

A similar design strategy was employed on the elevon itself, except a C_P constraint level of 0.15 was used instead of 0.2, based on C_P-SEP correlations for this area. As can be seen in Fig. 9a, the regions of weakened boundary layer and incipient separation have been significantly reduced (compared to Fig 6a). The stream-wise pressure and skin-friction changes were similar to those shown in Fig. 7b and 8a. It is believed that the shape of the new skin-friction distribution should delay the forward progression of separation as angle of attack or elevon deflection is increased.

As a check on the zonal design method, the new grids from all three zones were inserted back into the full grid and the flow solver was run starting from the baseline solution. As shown in Fig. 9, the flow on the elevon is slightly different, possibly due to circulation effects since the changes in that zonal design did not necessarily conserve lift. A full-grid analysis with the minmod limiter turned off for more accurate prediction of drag was also run, with the results indicating that the design had about a 1.3 per cent improvement in lift-to-drag ratio relative to the baseline. The pitching moment was also slightly less negative, which should provide a trim drag benefit.

E. CFD Elevon Evaluation

In addition to reducing the drag at cruise, one of the goals in improving the boundary layer characteristics on the elevon was to make the control surface more effective when deflected. Developing a new unstructured grid with elevon edges and gaps represented would have been the most accurate way to assess any improvement in elevon effectiveness for the new design, but a detailed geometry model for the design had not been developed from the final grid at that time. Since CDISC has a simple flap constraint option, it was decided to evaluate it even though the grid movement scheme would provide only a crude modeling of the elevon edges with no gaps. A shaded representation of the CFD model of the new design with the elevon deflected 5 degrees trailing-edge down is shown in Fig. 10. The boundary-layer-tailoring bumps developed in the design can also be seen ahead of the inlet.

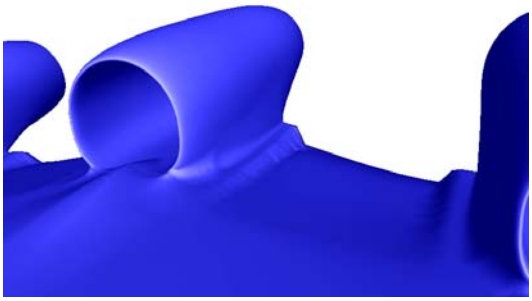

Figure 10 CFD modeling of elevon deflection.

F. Evaluation of Model Mounting System

The previous test of a wing-only BWB model in the NTF used a rear-mounted straight sting with a sting fairing as shown on Fig. 1. This approach would obviously not work for this case where the key region of interest is in the vicinity of the aft-mounted nacelles. Several other model support approaches were considered, including a yoke attached to the wing tips, a lower plate, and a lower swept strut or blade. A lower swept strut mounted toward the back of the model was considered for the previous NTF test, but CFD analysis indicated that the interference would significantly increase the strength of shocks on both the upper and lower surfaces. An examination of the lower surface pressures for the current configuration, however, revealed that the velocities there were fairly small over the forward half of the model centerline; thus, the superimposed velocities of the strut would be less likely to create strong shocks if the strut were mounted further forward.

This concept was evaluated using CFD for a wing-only (no nacelles) configuration and a sting geometry derived from an upper-strut mount that simulates the vertical tail on a conventional jet transport. The computations were performed using OVERFLOW with the S-A turbulence model. The wing-only grid had 6 zones with over 6 million

grid points, whereas the wing-strut cases had about twice as many zones and almost three times as many grid points. These initial computations indicated fairly low levels of interference, so a detailed definition of the actual strut geometry was developed and analyzed. A very weak shock was visible on the wing lower surface and the blade portion of the sting, but in general the interference appears to be very benign. Figure 11 shows the chord-wise pressure distributions at 3 span stations. As can be seen, the effects of the strut are fairly local, with almost no impact on the upper surface pressures. A number of runs at different angles of attack and Mach numbers were then made with the two configurations to develop corrections for sting effects to be applied to the wind tunnel data.

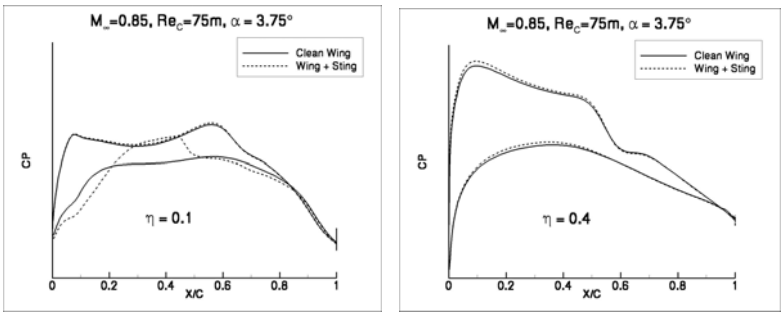

a) η=0.10 **b) η=0.40**

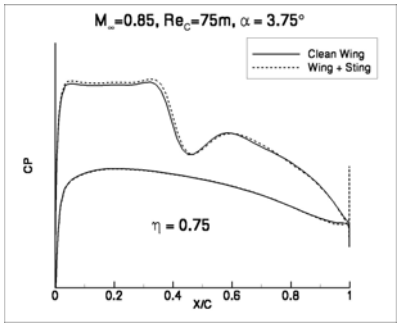

c) η=0.75

Figure 11 Comparison of stream-wise pressure distributions for the wing-only and wing-strut configurations at cruise conditions.

The predicted strut corrections for the lift, drag, and pitching-moment coefficients as a function of angle of attack are plotted in Fig. 12. The increments were converted into percentages of the wind tunnel data for the baseline BLI configuration at cruise. Also included on each plot is the linear approximation that was used to correct the wind tunnel data. Figure 12a shows the lift correction is nearly constant and less than 1 percent of the cruise lift coefficient. The drag correction varies more with angle of attack, but is still fairly linear. The approximately 3 percent correction at the cruise angle of attack (4 degrees) is similar to that of the rear-mounted sting used in the

original AST BWB test. The pitching moment correction is a larger percentage of the cruise value compared to the other force corrections. This is partly due to the small pitching moment at cruise since the aircraft is close to being trimmed. These corrections are also less linear than the lift or drag corrections. For performance comparisons between the baseline and redesigned BLI configurations at cruise, the linear estimate used for data reduction is adequate; however for accurate stability evaluations, a non-linear model and a broader angle of attack range of CFD results would be required.

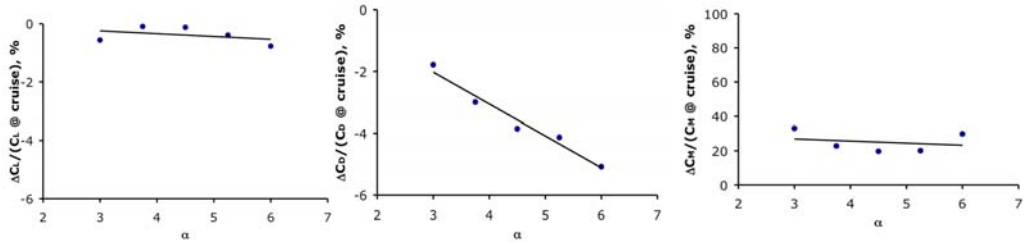

a) Lift **b) Drag** **c) Pitching moment**

Figure 12 Strut interference effects computed using OVERFLOW.

III. Wind Tunnel Test

A. Facility

An experimental evaluation of the BWB configurations was conducted in the National Transonic Facility (NTF) at the NASA Langley Research Center. The NTF is a pressurized, fan-driven, closed-circuit, continuous-flow wind-tunnel. The test section's cross-section is 8.2 by 8.2 ft, and has a length of 25 ft. The floor and ceiling of the test section are slotted (6 percent open), while the sidewalls are solid. The facility is able to operate in warm temperatures using dry air, or at warm to cryogenic conditions using nitrogen gas. The NTF can test at temperatures ranging from 150°F to –320°F, Mach numbers ranging from 0.2 to 1.2, absolute pressures ranging from 15 to 130 psi, and a maximum Reynolds number of 146×10^6 per foot at Mach 1.0.[23]

B. Model

The BWB model, a 2-percent scaled version of the 450-1L configuration, was designed to accommodate the testing goals of several research groups. In addition to the performance testing conducted under the UEET project, a stability and control test at NTF is scheduled . In order to meet the goals of both programs, the model was made with many interchangeable parts. There are four primary configurations: a clean wing (no nacelles), pylon-mounted

nacelles, and the baseline (Fig. 13) and redesigned BLI nacelles. The model has a total of 12 elevons that can be individually deflected. In addition, the wings can terminate in either a semicircular cross-section wing tip (Fig. 13) or a winglet.

Figure 13 Baseline BLI model configuration.

Since the goal of this wind tunnel test was to verify the predicted performance improvements for the new design relative to the baseline, the model was designed to interface with a blade sting (Fig. 14) to minimize any impact on the flow in the nacelle region. The blade connects to the balance that is attached to the model via a strut block that can be changed to allow testing at various yaw angles. For this test the yaw angle was held constant at zero degrees.

Figure 14 Lower swept-strut.

The model and sting were made out of a maraging steel and the model surface finish was 2–4 micro-inches. The model, including all the interchangeable parts, had over 400 pressure ports. Due to limited space within the model, only four electronically-scanned pressure (ESP) modules could be used. Consequently, only 248 pressure ports could be monitored at a time.

C. Test Conditions

The primary objective of the test was to evaluate the performance of the redesigned BLI nacelle configuration relative to the baseline geometry at realistic operating conditions (high Reynolds numbers, cruise Mach and angle of attack ranges). Given the size of the model, the maximum Reynolds number obtainable was 75 million (this is

roughly equivalent to the 25 million Reynolds number of the previous wing-only AST test when adjusted to the same reference chord). The cruise Reynolds number for the full-scale aircraft is approximately 180 million.

All four configurations, with semicircular cross-section wing tips and elevons at zero degrees, were tested at cryogenic conditions (–250°F), at Mach numbers ranging from 0.84 to 0.86, and angles of attack ranging from –1 to 8 degrees. The two BLI configurations were also tested with the two innermost elevons deflected 5 degrees (Fig. 15). Additionally, the clean wing configuration was tested at Mach numbers ranging from 0.5 to 0.88.

Figure 15 Deflected elevons (5-degrees).

The clean wing and pylon-mounted nacelle configurations with winglets were also tested in warm air (120°F). The clean wing was tested at Reynolds numbers of 10 and 16 million, Mach numbers ranging from 0.5 to 0.88, and angles of attack of –3 to 11 degrees. The configuration with pylon-mounted nacelles and winglets configuration was tested at Reynolds numbers of 2.4, 3.7, and 10 million, Mach numbers ranging from 0.2 to 0.9, and angles of attack from –3 to 16 degrees.

D. Repeatability and Data Uncertainty

In order to analyze the uncertainty of the data, the Mach 0.85 alpha sweep was repeated twice for each configuration. By conducting these sweeps at the beginning, middle, and end of each testing series any variances due to time were also captured. In order to provide a quantitative measure of uncertainty, the standard deviation was calculated from the repeat runs using

$$\sigma = R/d_{2,3}$$

where R is the mean range of the test data and $d_{2,3}$ is the mean range derived from a normal distribution with $\sigma=1$ for a sample of size of three ($d_{2,3} = 1.693$).[24]

Table 2 shows the uncertainty of the drag and moment data for the 75 million Reynolds number runs, with lift being held constant. This analysis showed the uncertainty to be minimal in the limited alpha sweep region of interest (angles of attack between 1 and 5 degrees). Since the balance was calibrated to obtain minute differences in drag,

when dynamics were encountered in the very low and high angles of attack, they caused severe fluctuations in that data, affecting the overall uncertainty of the data.

Configuration	Drag		Drag Counts		Moment	
	Overall	1-5 deg	Overall	1-5 deg	Overall	1-5 deg
Cleanwing	1.10E-04	2.685E-05	1.10	0.27	1.50E-04	6.531E-05
Baseline BLI Nacelles	2.494E-04	2.870E-05	2.49	0.29	1.979E-04	5.451E-05
Baseline 5-deg Elevons	8.557E-05	1.195E-05	0.86	0.12	1.445E-04	7.908E-05
Pylon-Mounted Nacelles	1.338E-04	8.246E-05	1.34	0.82	1.301E-04	9.329E-05
Redesigned BLI Nacelles	1.443E-04	1.826E-05	1.44	0.18	2.793E-04	6.690E-05
Redesign 5-deg Elevons	1.028E-04	3.366E-05	1.03	0.34	2.051E-04	9.843E-05

Table 2 Uncertainties of Experimental Data.

F. Data Comparisons

The remaining figures in this paper provide a series of comparisons of the CFD predictions with results from the wind tunnel tests[25]. Figure 16 compares the lift and moment curves of the baseline and redesigned BLI configurations with elevons at zero degrees. The lift curve for the redesign shifts slightly downward from the baseline. This shift along with the C_L values were accurately predicted by CFD.

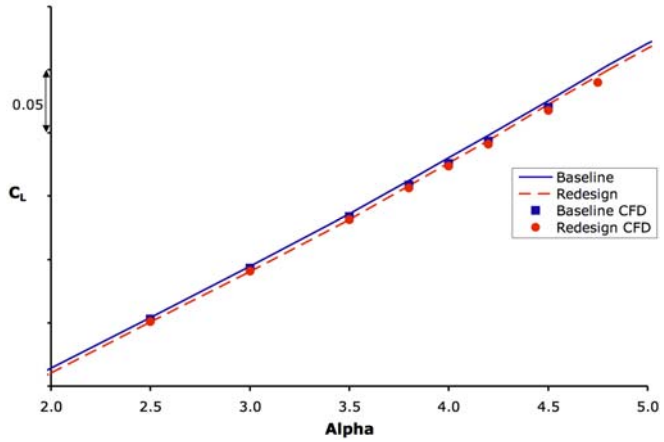

a) Lift Vs. Alpha

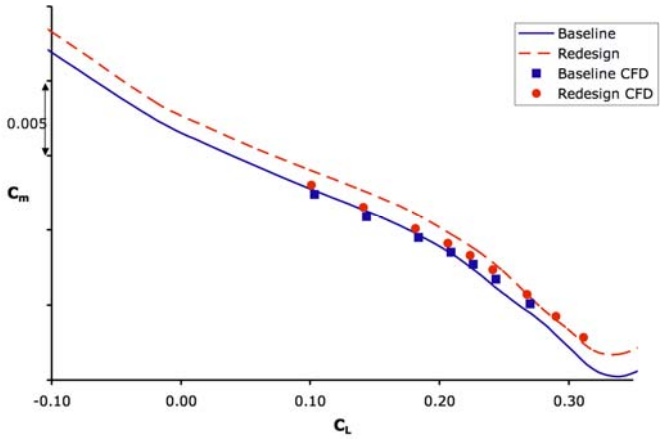

b) Pitching moment Vs. Lift

Figure 16 Wind Tunnel Vs. CFD curve comparisons.

Results for pitching moment show that the two configurations have very similar slopes at any given C_L, but the redesign curve shifts in the positive C_m direction relative to the baseline. This brings the redesign closer to trim at the cruise condition ($C_L = 0.24$), reducing the amount of elevon deflection needed to trim the aircraft thus reducing the trim drag. Although the CFD was able to match the experimental C_m at cruise conditions reasonably well, the pitch stability and the C_m increment between the baseline and redesign were under-predicted. This was not surprising since pitching moment is the most difficult component for CFD to predict accurately.

The lift vs. drag curve (Fig. 17a) shows that, up to the highest C_L computed for the baseline configuration, the redesign nacelles have reduced the drag. Over this region, CFD was able to predict the drag levels and increments reasonably well. Figure 17b shows the values of the drag reduction obtained by the redesign nacelles for a given C_L. The two lines surrounding the x-axis represent the uncertainty of the data. The results indicate that the wind tunnel data closely matched the predicted drag improvement of 1.3 percent for the redesign configuration.

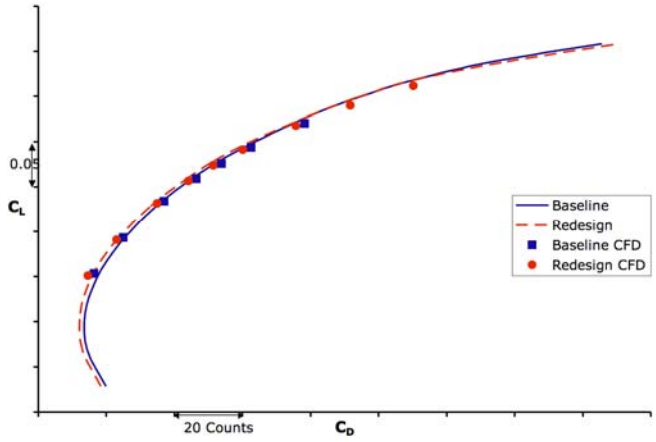

a) Lift vs. drag

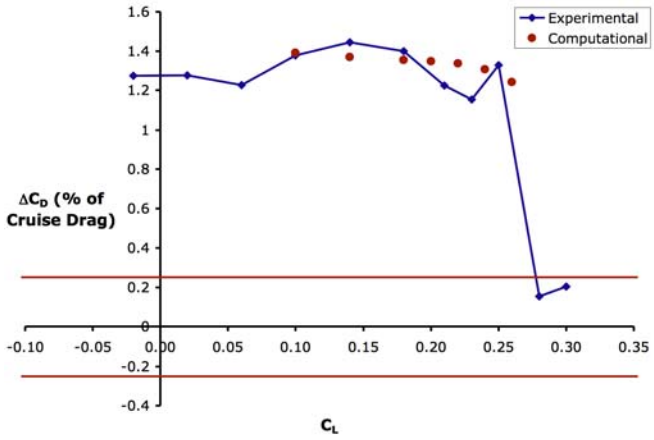

b) Drag Reduction

Figure 17 Wind Tunnel Vs. CFD Drag comparisons.

The modeling of the elevon deflection along with the elevon effectiveness was next examined. Figure 18 shows the change in L/D caused by a 5-degree elevon deflection. Overall, the deflection of the elevons produced a larger change in L/D on the redesign configuration than on the baseline, although at the cruise condition there is very little difference in the experimental data. The CFD predicted the increments between configurations and levels fairly well within the cruise range, but the correlation deteriorates for values of C_L away from cruise. The agreement between CFD and experiment seems to confirm that the simple modeling of the elevons in the CFD was adequate for examining overall forces and moments near cruise.

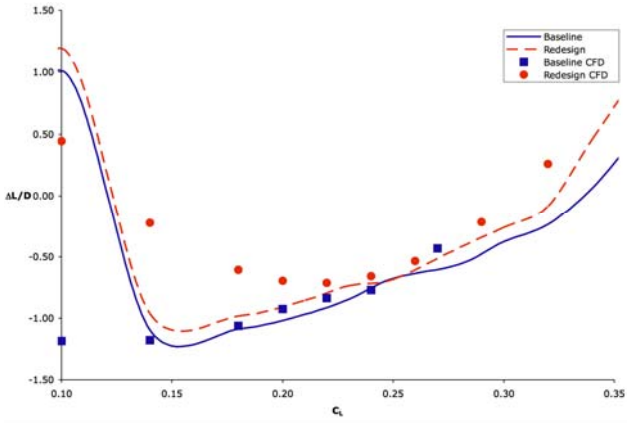

Figure 18 L/D increments for a 5-degree elevon deflection.

The elevon effectiveness data was combined with the overall shift of the C_m curve to estimate a trim drag benefit for the redesign configuration of about 0.8 percent. This brings the total drag reduction at cruise to about 2 percent.

While this is not a huge benefit, it is significant considering the limited area involved in the redesign and the very reasonable flow conditions (e.g., weak nacelle shocks) for the baseline. The increment is very similar to that achieved using numerical optimization[10], although the baseline configuration in that study had what appeared to be fairly strong shocks and significantly more flow channeling effects than in the current investigation.

A chordwise pressure distribution at cruise conditions of Mach 0.85, Reynolds number of 75 million, and an angle of attack of 4.2 degrees is shown in Fig. 19. This data location of η=0.10 goes through the middle of the elevon in between the two nacelles. The pressure distribution for the redesign matches the baseline distribution up to x/c=0.8, the location where the redesign changes begin. This indicates that, at least for this station, the redesign changes maintained the original level of circulation and thus tends to confirm the validity of the zonal design approach in this area. The CFD was able to predict the changes in the pressure gradients due to the redesign near the trailing edge seen in the experimental results.

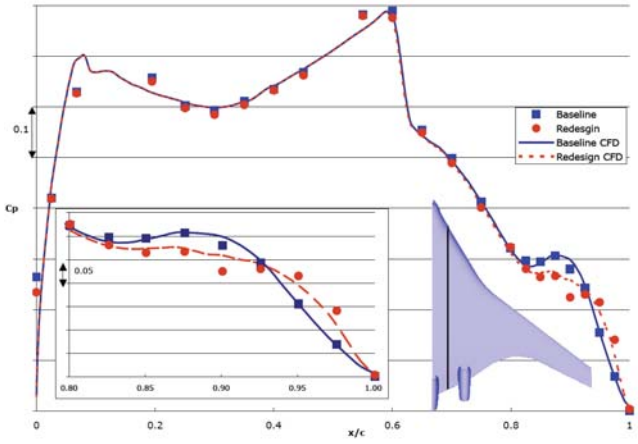

Figure 19 Comparison of C_P distribution at cruise conditions for η=.10.

IV. Concluding Remarks

The primary goal of this task within the UEET Project was to evaluate CFD design methods for use in propulsion/airframe integration and confirm their effectiveness through high-Reynolds number wind tunnel tests. During the course of this study, a number of conclusions and recommendations were developed relative to the CFD and the wind tunnel testing aspects of the project. The USM3D flow solver was shown to be sufficiently accurate for use in design, with good correlation demonstrated between its predictions and wind tunnel data from a previous BWB test in the NTF as well as the results of the current PAI tests. Particularly encouraging was the verification of

fairly small changes in drag and local pressures between the baseline and design configurations. Elevon deflection effects were also predicted fairly well even though a crude grid model was used in the CFD. The unstructured grid approach used by USM3D simplified the implementation of the CDISC design methodology for this fairly complex geometry, eliminating the need to generate lengthy projection scripts required for overset unstructured grids. In addition, the zonal design capability significantly reduced the time required to develop a successful design strategy, in one case providing a factor of 20 savings in time and memory relative to using the full grid.

In regard to the high-Reynolds number testing in NTF, the results confirmed the predicted design benefits. Balance and pressure instrumentation accuracies were well within the levels required to capture the small design changes, and repeatability between runs was good. Because a sensitive balance was required to achieve this level of accuracy, there were some run conditions that could not be obtained due to model dynamic loads. While this did not impact the primary objectives of this test, it may be a concern for future stability and control testing. Even though the pressure instrumentation was fairly extensive in the region of the nacelles, more detail was needed to fully assess a PAI design.

References

[1] Liebeck, R, "Design of the Blended-Wing-Body Subsonic Transport," AIAA-2002-0002, January 2002.

[2] Daggett, David L., Kawai, Ron, and Friedman, Doug, "Blended Wing Body Systems Studies: Boundary Layer Ingestion Inlets With Active Flow Control," NASA CR-2003-212670, December 2003.

[3] Roman, D., Allen, J. B., and Liebeck, R. H., "Aerodynamic Design Challenges of the Blended-Wing-Body Subsonic Transport," AIAA-2000-4335, August 2000.

[4] Holmes, Stanley, "The Battle over a Radical New Plane," *Business Week*, Vol. 145, November 25, 2002, pp. 106-108.

[5] Clark, Lorenzo R., and Gerhold, Carl H., "Inlet Noise Reduction by Shielding for the Blended-Wing-Body Airplane," AIAA-99-1937, May 1999.

[6] Rodriguez, David L.,"A 3D Multidisciplinary Design Method for Designing Boundary Layer Ingesting Inlets," AIAA-2000-0424, January 2000.

[7] Rodriguez, David L.,"A Multidisciplinary Optimization Method for Designing Boundary Layer Ingesting Inlets," AIAA-2002-5665, September 2002.

[8] Gorton, Susan Althoff, Owens, Lewis R,, Jenkins, Luther N., Allen, Brian G., and Schuster, Ernest P., "Active Flow Control on a Boundary-Layer-Ingesting Inlet," AIAA-2004-1203, January 2004.

[9] Allan, Brian G., Owens, Lewis R., and Berrier, Bobby L., "Numerical Modeling of Active Flow Control in a Boundary Layer Ingesting Offset Inlet," AIAA-2004-2318, July 2004.

[10] Pelkman, Regina A., "Key Findings & Conclusions from an NTF Wind Tunnel Test of an Initial Blended-Wing-Body Concept," NASA Contract NAS1-20268, TR-3985, August 1998.

[11] Campbell, Richard L., "Efficient Viscous Design of Realistic Aircraft Configurations," AIAA-98-2539, June 1998.

[12] Jespersen, D.C., Pulliam, T.H., and Buning, P.G., "Recent Enhancements to OVERFLOW," AIAA-97-0644, January 1997.

[13] Frink, N.T., "Assessment of an Unstructured-Grid Method for Predicting 3-D Turbulent Viscous Flows," AIAA-96-0292, January 1996.

[14] Frink, N.T., Pirzadeh, S.Z., Parikh, P.C., Pandya, M.J., and Bhat, M.K., "The NASA Tetrahedral Unstructured Software System," *The Aeronautical Journal*, Vol. 104, No. 1040, October 2000, pp.491-499.

[15] Nielsen, Eric J., and Anderson, W. Kyle, "Recent Improvements in Aerodynamic Design Optimization On Unstructured Meshes," AIAA 2001-0596, January 2001.

[16] Re, Richard J., "Longitudinal Aerodynamic Characteristics and Wing Pressure Distributions of a Blended-Wing-Body Configuration at Low and High Reynolds Numbers, NASA TM-2005-213754, August 2005.

[17] Roe, P., "Characteristic Based Schemes for the Euler Equations," *Annual Review of Fluid Mechanics*, Vol. 18, 1986, pp. 337-365.

[18] Spalart, P., and Allmaras, S.A., "One-equation turbulence model for aerodynamic flows," AIAA 92-0439, January 1992.

[19] Menter, F.R., "Improved Two-Equation k-omega Turbulence Models for Aerodynamic Flows," NASA TM-103975, October 1992.

[20] Pirzadeh, S., "Three-Dimensional Unstructured Viscous Grids by the Advancing-Layers Method," *AIAA Journal*, Vol. 34, No. 1, January 1996, pp.43-49.

[21] Carter, Melissa Beth, "A computational Investigation of the Design Techniques for Propulsion Airframe Integration on a Blended Wing Body," Masters Thesis, School of Engineering and Applied Science, George Washington University, Washington DC, May 2004.

[22] Green, Bradford E., and Whitesides, John L., "Method for Designing Leading-Edge Fillets to Eliminate Flow Separation," *Journal of Aircraft*, Vol. 40, No. 2, March-April, 2003, pp. 282-289.

[23] Wahls, R., "The National Transonic Facility: A Research Retrospective," AIAA-2001-0754, January 2001.

[24] Hemsch, M., "Statistical Analysis and Characterization of NTF Repeatability Tests: Flow Angularity," AIAA-2006-0518, January 2006.

[25] Campbell, R., Carter, M., Pendergraft, O., Friedman, D., and Serrano, L., "Design and Testing of a Blended Wing Body with Boundary Layer Ingestion Nacelles at High Reynolds Numbers (Invited)," AIAA-2005-0459, January 2005.